Proceedings of the 16th International Heat Transfer Conference, IHTC-16
August 10-15, 2018, Beijing, China

IHTC16-23328

A STUDY OF THE EFFECTS OF THE PORE SIZE ON TURBULENCE INTENSITY AND TURBULENCE LENGTH SCALE IN FORCED CONVECTION FLOW IN POROUS MEDIA

Ching-Wei Huang[1], Timothy S. Su[1], Vishal Srikanth[1], Andrey V. Kuznetsov[1*]

[1] Department of Mechanical and Aerospace Engineering, North Carolina State University, Raleigh, North Carolina 27695-7910, USA

ABSTRACT

We investigated the relation between the pore size and turbulence intensity for flows in porous media. Our goal was to address a paradox between turbulence generation by a single solid obstacle and turbulence suppression by multiple solid obstacles. In a clear fluid region, a single obstacle will act as a turbulence enhancer, with the enhancement being proportional to the obstacle size. Unlike around a single obstacle, turbulence in a porous medium is restricted by the surfaces of other obstacles surrounding it. This restriction is expected to be proportional to the distance between the surfaces of the two neighboring obstacles.

We used a representative elementary volume (REV) with 4×4 cylindrical obstacles to represent the infinite porous medium structure. The REV had periodic boundaries in the *x*, *y* and *z*-directions, and a specified mass flow rate in the *x*-direction. Changing the cylinder diameter, *d*, under a constant Reynolds number of approximately 5,000, we compared the macroscopic turbulence intensity, $I_{t,macro}$, the location of maximum turbulence intensity, $I_{t,max}$, and the maximum turbulence length scale, $l_{t,max}$, for each case. Although the driving force (the applied pressure gradient) acts only in the *x*-direction, we observed a mean velocity in the *y*-direction, and a noticeable change in the bulk flow direction for the $d/s = 0.8$ case, where *s* is the distance between centers of the obstacles. We found that $I_{t,macro}$ increases in the range $d/s = 0.1\sim0.4$ with increased *d*, then slightly decreases in the range $d/s = 0.6\sim0.8$. We think this is caused by the turbulence suppression from cylinder walls. We also observed the bulk flow direction deviating from the direction of the applied pressure gradient, which could also contribute to the slight decrease of $I_{t,macro}$ in these cases. The location of $I_{t,max}$ changes from near the separation point slightly behind each cylinder for $d/s = 0.1\sim0.2$, to the location where the wake comes into contact in the front of each cylinder for $d/s = 0.4\sim0.8$. This suggests that the turbulence generated by a cylinder is being suppressed by the surrounding cylinders. The maximum turbulence length scale decreases with increased *d* throughout the range of $d/s = 0.1\sim0.8$. There is a large decrease in the range $d/s = 0.1\sim0.2$, which we believe is the result of turbulence structures generated from each cylinder starting to interact with the surrounding cylinders.

Although further confirmation of these results is required, this study provides an estimate on how the pore size may affect the turbulent flow in porous media with large solid obstacles.

KEY WORDS: Porous medium, Pore size, Turbulence, Turbulence intensity, Turbulence length scale

*Corresponding Author: avkuznet@ncsu.edu

1. INTRODUCTION

Flows in a porous media is an important area of study due to the wide range of its applications, including heat exchanger design, filter efficiency prediction, and biomechanics of kidney and liver [1]. One of the important topics for flows in porous media is whether macroscopic turbulence, characterized by turbulent structures larger than the pore size, can exist in a porous medium [2].

The modeling of turbulence in porous media, based on both pore-scale turbulence and large-scale turbulence, has been reviewed by de Lemos [3] and more recently by Nield and Bejan [1]. Models that relied on a large-scale (macroscale) turbulence approach were developed by Lee and Howell [4], Prescott and Incropera [5], Antohe and Lage [6] as well as by other researchers. Nield [7,8] suggested that the pore scale could limit the size of turbulent eddies. Recent studies by Jin et al. [2], Uth et al. [9], and Jin and Kuznetsov [10] used Direct Numerical Simulation (DNS) of forced convection flows in porous media which suggested that the pore size of the porous medium determines the maximum size of turbulent eddies. Due to the restriction on the size of turbulent eddies, turbulent kinetic energy is unable to transfer from larger to smaller turbulent eddies. This in turn prevents large scale turbulence. This suggests that turbulence in a porous medium, due to its much smaller intensity, acts differently from turbulence in a clear fluid. For the case of a bidispersed porous medium, characterized by two significantly different pore scales, there may even be a second critical Reynolds number. It is possible that, when involving flows in composite porous/fluid domains, a flow in a porous region may be approximated as laminar even though a flow in a clear fluid region is turbulent [11,12].

To further understand the effects of porous media on turbulent flows and to better understand the relation between the pore scale and turbulence intensity, we compared flows in porous media with different pore sizes. We discuss the change in the distribution of turbulence intensity as well as changes in the flow field pressure and velocity distributions caused by the change in the pore size. The Reynolds number that describes the pore-scale turbulence should be dependent on a certain characteristic length of the porous medium geometry. This length is likely to be the hydraulic diameter of the pore cross section if we treat the flow as an internal flow, or the distance between the obstacles' surfaces if we view it as an external flow.

2. METHODS

2.1 Geometry In order to simulate an infinite periodic matrix, we used a representative elementary volume (REV). This is the smallest sub-volume that shows the same behavior as the flow in the whole porous domain. The size of the REV is chosen considering the paper by Uth et al. [9]. In the paper they reported that the largest scale of a turbulence structure observed in their DNS study was approximately four times the distance between centers of the obstacles, s. Thus, we will assume that using a REV with a side length of $4s$ will be sufficient to capture how the turbulence behavior is affected by the change in the diameter of the cylindrical obstacles.

The size of the REV is $4s \times 4s \times 2s$ in the x, y, and z-directions respectively, as shown in Fig. 1. The REV consists of 4×4 cylindrical obstacles whose center points are a distance s apart in the x and y-directions. In our computations, the diameter of the cylinder d is varied from $0.1s$ to $0.8s$. The porosity, φ, for this geometry is calculated as

$$\varphi = 1 - \frac{\pi}{4}\left(\frac{d}{s}\right)^2 \tag{1}$$

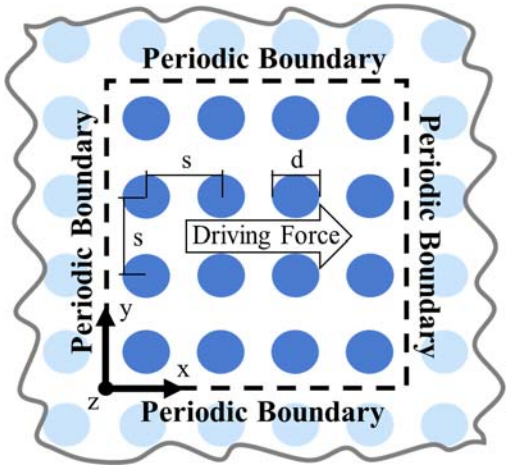

Fig. 1 The representative elementary volume (REV) geometry of a porous medium with an infinite number of cylindrical obstacles.

2.2 Boundary Conditions Periodic boundary conditions were used in the *x*, *y* and *z*-directions, respectively, with a specified mass flow rate, $\dot{m}$, in the *x*-direction to keep the Reynolds number constant. No-slip boundary conditions were used on the walls of the cylindrical obstacles.

2.3 Models The turbulence model used in this study is the realizable *k*-*ε* model. Computations were performed using the commercial software ANSYS FLUENT 18.1 (ANSYS, Canonsburg, Pennsylvania) [13]. The velocity u was represented as a combination of the mean velocity, $\bar{u}$, and the unsteady fluctuation velocity, u':

$$u = \bar{u} + u' \tag{2}$$

where $\bar{u}$ was calculated from the three mean velocity components in the *x*, *y*, and *z*-directions and $u'$was calculated by the root-mean-square of the turbulent velocity fluctuations. To investigate the effect of the obstacle size on turbulence, we compared the turbulence intensity, I_t, the macroscopic turbulence intensity, $I_{t,macro}$, and the turbulence length scale, l_t, defined as:

$$I_t = \frac{u'}{\bar{u}} \tag{3}$$

$$I_{t,macro} = \frac{\sqrt{2\langle k \rangle}}{\langle U \rangle} \tag{4}$$

$$l_t = 0.09^{\frac{3}{4}} \frac{k^{\frac{3}{2}}}{\varepsilon} \tag{5}$$

where k is the turbulence kinetic energy and ε is the turbulence dissipation rate calculated from the realizable *k*-*ε* model. $\langle k \rangle$ and $\langle U \rangle$ are the volume averaged values of turbulence kinetic energy and velocity magnitude, respectively.

2.3 Validation and Accuracy To validate our simulation results, we compared our computational data for the drag coefficient C_d for a flow over a single cylinder, obtained using the same meshing, geometric and boundary conditions as for the REV, with experimental data for a flow over a single cylinder [14]. This allowed us to verify that the model is capable to accurately predict the boundary layer flow around the cylinder, as well as the drag force between the surface of the cylinder and the flow.

A large eddy simulation (LES) was preformed to verify and further examine the results for the $d/s = 0.8$ case.

3. RESULTS AND DISCUSSION

3.1 Velocity Distribution To minimize errors caused by the boundary conditions, we presented data on the plane $z = 0.5s$. We maintained a constant Reynolds number of 5,000 by specifying an *x*-direction mass flow rate in the boundary conditions. This Reynolds number determines the mean *x*-direction velocity of the flow field, U_x. The corresponding porosity for each case is shown in Table 1.

In the $d/s = 0.2{\sim}0.4$ cases, as shown in Fig. 2(a) (b), the flow around the rows of cylinders in the *x*-direction barely interacts with the flow around neighboring rows. This forms a "duct"-like region between the two rows of cylinders in the *x*-direction. The vortices in the wake behind a cylinder are attached to the cylinder's wall. The vortex core size is not restricted by the next cylinder in the *x*-direction, and the flow field is generally symmetric.

For larger cylinders ($d/s = 0.6{\sim}0.8$), the vortices behind the cylinders propagate at an angle to the principle flow direction, forming a mean velocity in the *y*-direction. The mean *y*-velocity can be directed upward or downward; these two cases are analogous. Consider the situation where the mean *y*-velocity is directed upward. This aids in the identification of the top and bottom half of the cylinder. Our LES results for the $d = 0.8s$ case suggest that the change in the bulk flow's direction is caused by the pressure gradient from the diverging and converging walls of the cylinders. This pressure gradient forces the shedding vortices that are first formed in the developing stage of the flow to recirculate and break down into smaller vortices. After the von Karman instability is formed, it creates an uneven shedding of the vortices behind these cylinders. These uneven vortices interact with the recirculating vortices that have broken down and form uneven vortices on the top and bottom side behind the cylinder. This creates a pressure difference between the uneven vortices, driving the flow in the *y*-direction.

In the $d/s = 0.8$ case, as shown in Fig. 2(d), we observed the bulk flow deviating from the principle flow direction significantly (~30°). Iacovides et al. [15] reported a similar deflection of the flow over in-line tube banks. In this case the distance between the bottom separation point and the stagnation point on the horizontally adjacent cylinder is smaller, causing the bottom side separation point to be shifted downstream by the high pressure region near the stagnation point. This keeps the bottom side separation point near the throat formed by two horizontally aligned cylinders, resulting in a significant increase of the mean velocity in the *y*-direction. The mean *y*-velocity for various d/s ratios is reported in Table 1. The LES result for the $d/s = 0.8$ case is shown in Fig. 3, where we can see the formation of the flow field.

Table 1 Computational results for the mean velocity and porosity.

d/s	0.1	0.2	0.4	0.6	0.8
φ	0.992	0.968	0.874	0.717	0.497
U_y/U_x	3.27E-05	2.90E-05	4.29E-04	2.50E-01	6.78E-01

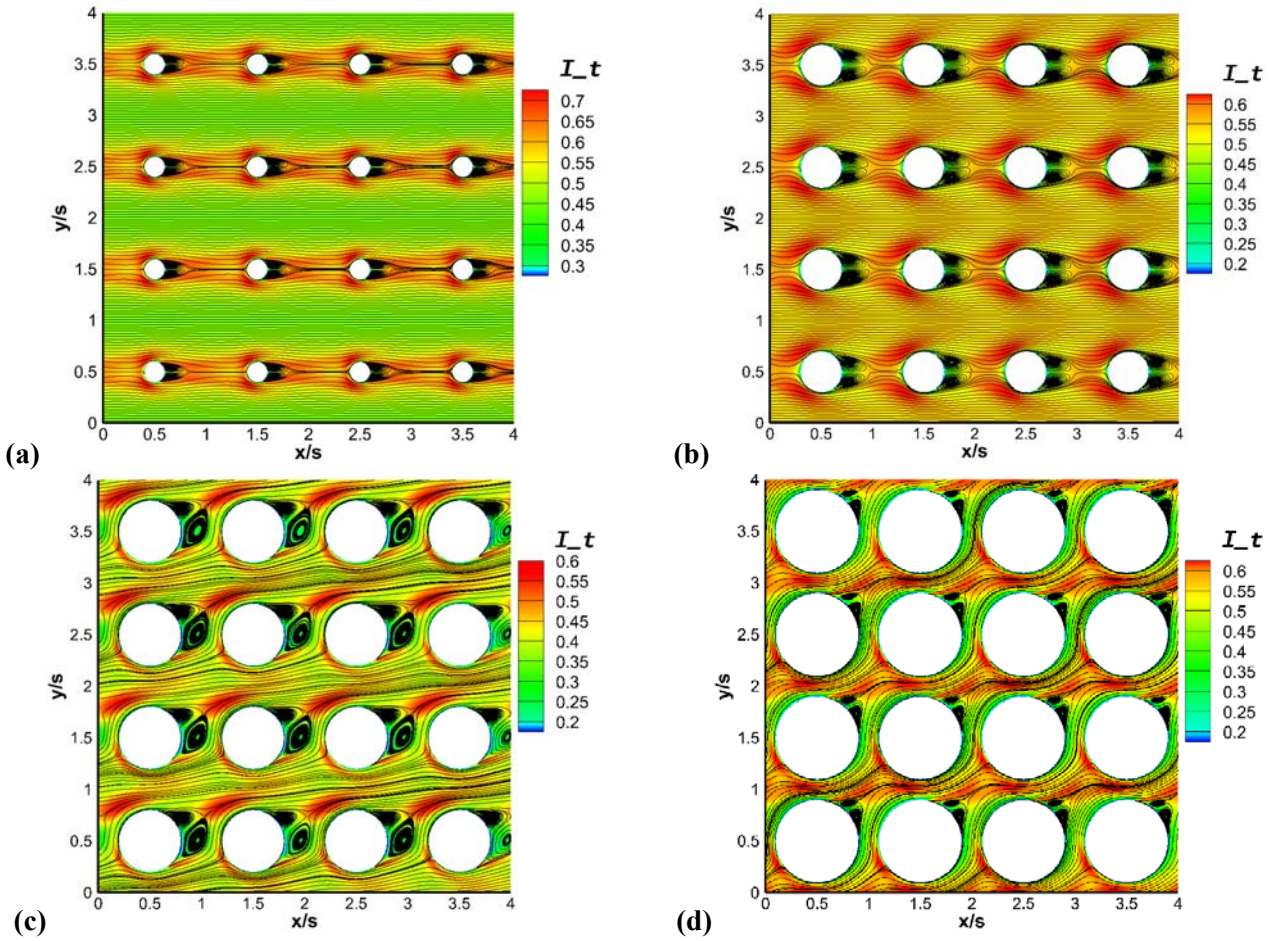

Fig. 2 Streamlines and turbulence intensity distributions in the REV. (a) $d/s = 0.2$; (b) $d/s = 0.4$; (c) $d/s = 0.6$; (d) $d/s = 0.8$.

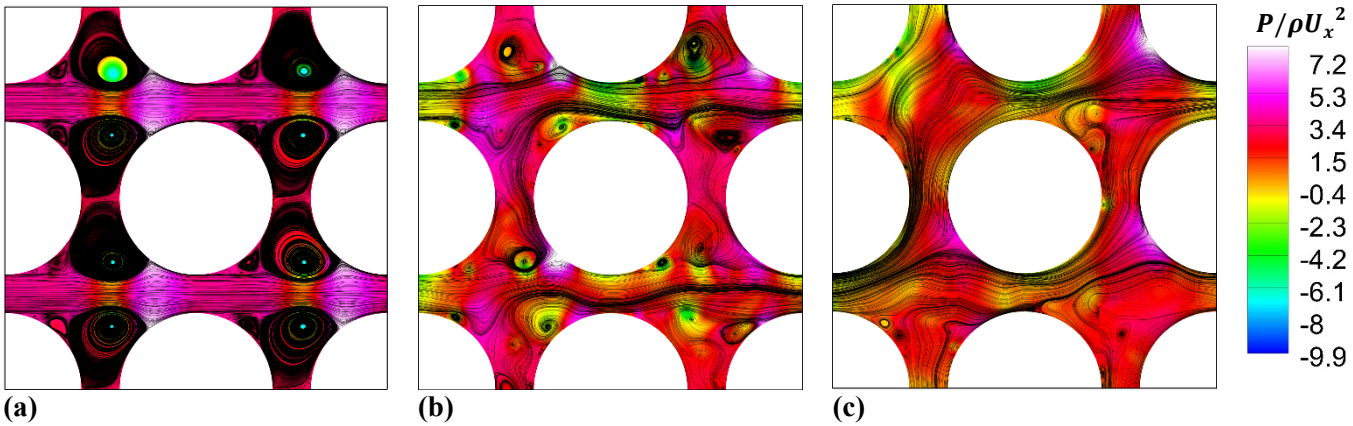

Fig. 3 Streamlines and pressure contour obtained from LES results of $d/s = 0.8$ case, showing the formation of the change in the bulk flow direction. (a) High pressure gradient from converging walls between two cylinders forces the shedding vortices to recirculate; (b) Uneven vortices form a pressure gradient, which drives the flow in the y-direction; (c) Delayed bottom separation point and change in the bulk flow direction.

3.2 Turbulence Intensity The simulation results show that for $d/s = 0.1\sim0.4$, the macroscopic turbulence intensity, $I_{t,macro}$, increases with increased d, and then slightly decreases in the range $d/s = 0.4\sim0.8$, as shown in Fig. 4(a). This agrees with our assumption that the obstacles promote turbulence, but the walls of surrounding obstacles act as a restriction of turbulence in the flow. The bulk flow deviating from the driving force direction could also contribute to the slight decrease in $I_{t,macro}$ for $d/s = 0.6\sim0.8$.

By comparing the contours of the turbulence intensity I_t for different cases in Fig. 2, we can see that the location of the maximum turbulence intensity, $I_{t,max}$, changes for different porosities. For $d/s = 0.1\sim0.2$, the location of $I_{t,max}$ is near the separation points behind each cylinder, as shown in Fig. 2(a). For $d/s = 0.4$, the location of $I_{t,max}$ changes to where the wake impinges on the front of the cylinder, and the magnitude of turbulence intensity near the separation point becomes relatively low, as shown in Fig. 2(b). This shows that the cylinder wall downstream is suppressing the turbulence of the shedding vortices from the cylinder upstream. As the mean velocity in the *y*-direction starts to appear at $d/s = 0.6$, the location of $I_{t,max}$ shifts downstream of the shedding vortices' path, as shown in Fig. 2(c). Due to deviation in the flow direction, the shedding vortices can dissipate in the flow, which decreases turbulence suppression by the downstream cylinder. This can be seen from the magnitude of I_t near the lower separation point increasing and becoming comparable to $I_{t,max}$. After a significant change in the mean flow direction, in the $d/s = 0.8$ case (Fig. 2(d)), the shedding vortices again impinge on the front of the cylinder downstream, suppressing the turbulence of the wake, and decreasing the magnitude of I_t near the lower separation point. These changes in the I_t distribution for different porosities suggest that the obstacle simultaneously generates turbulence and suppresses turbulence generated by the other obstacles.

3.3 Turbulence Length Scale Comparing the maximum turbulence length scale, $l_{t,max}$, for each case, we can see that $l_{t,max}$ first decreases with increasing d in the range $d/s = 0.1\sim0.2$ and then remains approximately constant in the range $d/s = 0.2\sim0.4$ (Fig. 4(b)). It then decreases with the increasing obstacle diameter until $d/s = 0.8$. These results agree with our hypothesis that $l_{t,max}$ is restricted by the surfaces of the neighboring obstacles. We think the first drop in $l_{t,max}$ in the range $d/s = 0.1\sim0.2$ is caused by the downstream cylinder starting to interact with the wake from the upstream cylinder in a horizontal row. Then in the range $d/s = 0.2\sim0.4$, the vortices that are dissipated on the downstream cylinder wall start to affect the "duct" flow region between two rows of cylinders. The effect slightly increases the turbulent kinetic energy and balances out the increased restriction from the walls, resulting in $l_{t,max}$ staying relatively constant. In the range $d/s = 0.6\sim0.8$, because of the change in bulk flow direction, the vortices behind a cylinder dissipate in the bulk flow instead of on the downstream cylinder wall. The vortices also become smaller as d grows larger, generating less turbulent kinetic energy. We can also see that $l_{t,max}$ continues to be restricted by the surfaces of neighboring obstacles.

We conclude that a value of d/s at which the turbulence length scale takes on its maximum value $l_{t,max}$ occurs before the obstacle walls start to restrict the size of turbulence structures, which happens before $d/s = 0.2$.

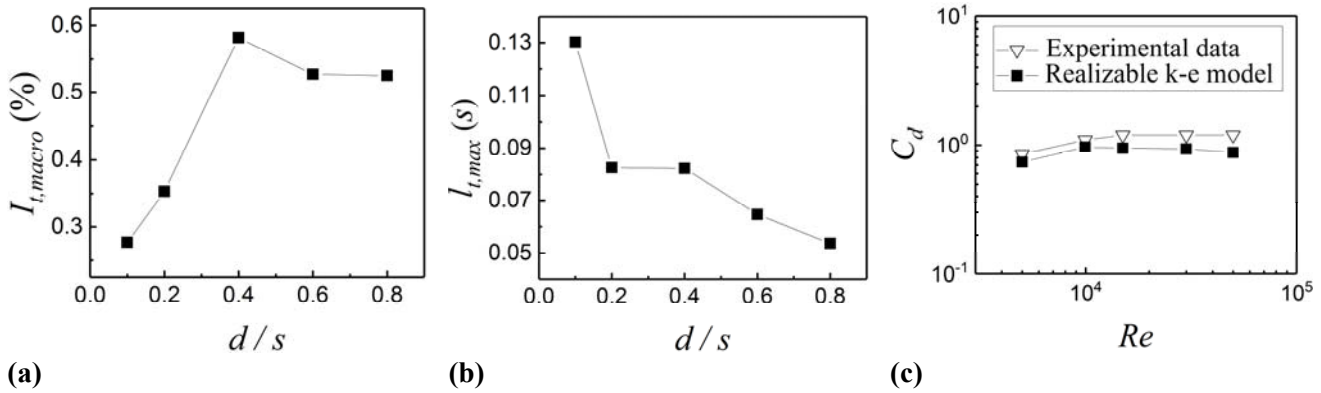

Fig. 4 (a) Turbulence intensity variation with the change in the diameter of the cylindrical obstacle, characterized by d/s; (b) Turbulence length scale variation with the change in the cylindrical obstacle diameter, characterized by d/s; (c) Comparison of the drag coefficients for flow over a single cylinder obtained computationally by using a realizable k-ε model and the experimental data of Panton et al. [14].

3.4 Drag Coefficient Comparison By controlling the mass flow rate, we used five different Reynolds numbers for the comparison: 5,000; 9,950; 15,000; 30,000; and 50,000. From these results, we can see that when the Reynolds number increases, the drag coefficient becomes almost constant. This is similar to the behavior of the experimental data, as shown in Fig. 4(c).

The results show that our simulation slightly underpredicts the drag acting on the cylindrical surface. This deviation may be caused by insufficient mesh resolution or by the utilization of a realizable k-ε model. We will modify the meshing and compare the simulation results of other models to improve the accuracy in future studies.

4. CONCLUSIONS

We used the realizable k-ε model to simulate a turbulent flow in a porous medium. By analyzing the turbulence intensity and turbulence length scale, we can see that the results support our hypothesis, first expressed in Jin et al. [2], which states that the turbulence length scale is restricted by the surfaces of the surrounding obstacles. The turbulence length scale thus should be comparable to the pore size. We also observed an interesting phenomenon in low porosity cases of $\varphi \leq 0.717$ ($d/s = 0.6{\sim}0.8$), where the bulk flow direction deviates from the driving force direction, and the flow becomes non-symmetric, even though the boundary conditions and geometry are symmetric. Although further confirmation of these findings is required, this study provides an estimate of how the pore size may affect turbulent flow in a porous medium.

The physics and parameters that control the observed change in the bulk flow direction at low porosities will be studied further in future research. Simulations of flows in porous media with a constant mass flow rate and different obstacle shapes will also be of interest for future studies. More DNS and LES studies are required to further confirm the obtained results.

ACKNOWLEDGMENT

AVK acknowledges with gratitude the support of the National Science Foundation (award CBET-1642262) and the Alexander von Humboldt Foundation through the Humboldt Research Award.

NOMENCLATURE

φ	porosity	(-)
g_p	pressure gradient	(Pa/m)
$\bar{u}$	mean velocity	(m/s)
u'	velocity fluctuation	(m/s)
I_t	turbulence intensity	(-)
l_t	turbulence length scale	(m)
k	turbulence kinetic energy	(m^2/s^2)
ε	turbulence dissipation rate	(m^2/s^3)
$\langle k \rangle$	volume averaged turbulence kinetic energy	(m^2/s^2)
$\langle U \rangle$	volume averaged velocity magnitude	(m/s)
U_x	mean *x*-velocity	(m/s)
U_y	mean *y*-velocity	(m/s)

Subscripts

s	distance between centers of neighboring cylinders	(m)
d	cylinder diameter	(m)
u	velocity	(m/s)

REFERENCES

[1] Nield, D. A., and Bejan, A., *Convection in Porous Media*, Springer International Publishing, (2017).

[2] Jin, Y., Uth, M.-F., Kuznetsov, A. V., andHerwig, H., "Numerical Investigation of the Possibility of Macroscopic Turbulence in Porous Media: A Direct Numerical Simulation Study," J. Fluid Mech., 766, pp. 76–103, (2015).

[3] Lemos, M. J. S. de., *Turbulence in Porous Media : Modeling and Applications*, Elsevier, (2012).

[4] Kum-Bae, L., andHowell, J. R., "Theoretical and Experimental Heat and Mass Transfer in Highly Porous Media," Int. J. Heat Mass Transf., 34(8), pp. 2123–2132, (1991).

[5] Prescott, P. J., andIncropera, F. P., "The Effect of Turbulence on Solidification of a Binary Metal Alloy With Electromagnetic Stirring," J. Heat Transfer, 117(3), p. 716, (1995).

[6] Antohe, B. V., andLage, J. L., "A General Two-Equation Macroscopic Turbulence Model for Incompressible Flow in Porous Media," Int. J. Heat Mass Transf., 40(13), pp. 3013–3024, (1997).

[7] Nield, D. A., "The Limitations of the Brinkman-Forchheimer Equation in Modeling Flow in a Saturated Porous Medium and at an Interface," Int. J. Heat Fluid Flow, 12(3), pp. 269–272, (1991).

[8] Nield, D. A., "Alternative Models of Turbulence in a Porous Medium, and Related Matters," J. Fluids Eng., 123(4), p. 928, (2001).

[9] Uth, M.-F., Jin, Y., Kuznetsov, A.V., andHerwig, H., "A Direct Numerical Simulation Study on the Possibility of Macroscopic Turbulence in Porous Media: Effects of Different Solid Matrix Geometries, Solid Boundaries, and Two Porosity Scales," Phys. Fluids, 28(6), p. 065101, (2016).

[10] Jin, Y., and Kuznetsov, A.V., "Turbulence Modeling for Flows in Wall Bounded Porous Media: An Analysis Based on Direct Numerical Simulations," Phys. Fluids, 29(4), p. 045102, (2017).

[11] Kuznetsov, A. V., "Numerical Modeling of Turbulent Flow in a Composite Porous/Fluid Duct Utilizing a Two-Layer K–ε Model to Account for Interface Roughness," Int. J. Therm. Sci., 43(11), pp. 1047–1056, (2004).

[12] Kuznetsov, A. V., "What We Can Learn from Direct Numerical Simulation of Turbulence in Porous Media : Modeling Turbulent Flow in Composite Porous/Fluid Domains," *Proc. of 13th International Conference on Heat Transfer, Fluid Mechanics and Thermodynamics,* pp. 932–939, (2017).

[13] A.N.S.Y.S. Inc, *ANSYS Fluent User's Guide*, (2017).

[14] Panton, R. L., *Incompressible Flow*, John Wiley & Sons, Inc., Hoboken, NJ, USA, (2013).

[15] Iacovides, H., Launder, B., andWest, A., "A Comparison and Assessment of Approaches for Modelling Flow over In-Line Tube Banks," Int. J. Heat Fluid Flow, 49, pp. 69–79, (2014).